J Nanopart Res (2012) 14:1200
DOI 10.1007/s11051-012-1200-2

RESEARCH PAPER

Spectroscopic and microscopic investigation of gold nanoparticle nucleation and growth mechanisms using gelatin as a stabilizer

Yi-Cheng Wang · Sundaram Gunasekaran

Received: 28 June 2012 / Accepted: 10 September 2012

Abstract A microscopic and spectroscopic investigation of the synthesis of gold nanoparticles (AuNPs) within gelatin is reported. The AuNPs were synthesized first by reducing tetrachloraurate ions ($AuCl4^-$) by 2-[4-(2-hydroxyethyl)-1-piperazinyl] ethanesulfonic acid (HEPES), mixing the $HAuCl_4$/HEPES solution with gelatin solution and heating at different temperatures. The polymeric structure of gelatin stabilized the $HAuCl_4$/HEPES/gelatin system and slowed the synthesis of AuNPs, enabling a time-dependent investigation. Based on the results of transmission electron microscopy (TEM) analysis and UV–Vis spectra, we identified three distinct stages involved in the synthesis of AuNPs. First, during the initial stage, the reduction of gold precursor occurred along with nucleation and growth, which resulted in a red-shift phenomenon of the localized surface plasmon resonance (LSPR) peak of AuNPs in UV–Vis spectra (size and size dispersion increase). Second, the LSPR peaks showed red-shift first and then blue-shift during the growth of AuNPs. The blue-shift might result from the diffusion-limited Ostwald-ripening mechanism. Third, as the supply of the growth species became lower, during the growth of AuNPs, a diffusion-limited Ostwald-ripening mechanism along with a blue-shift only phenomenon in UV–Vis spectra was observed. We also determined that slowing the synthesis process during the nucleation stage can prolong the nucleation time, which can generate larger AuNPs. The TEM analysis showed that higher heating temperature and longer heating time can lead to larger particles. By controlling the reduction (nucleation) time, heating time and temperature, AuNPs of size ranging from 5 to 17 nm can be synthesized.

Keywords Gold nanoparticles · HEPES · Gelatin · Nucleation · Temperature-dependent growth · Diffusion-controlled Ostwald-ripening mechanism

Y.-C. Wang · S. Gunasekaran (✉)
Department of Biological Systems Engineering, University of Wisconsin-Madison, 460 Henry Mall, Madison, WI 53706, USA
e-mail: guna@wisc.edu

Y.-C. Wang
Department of Chemistry, University of Wisconsin-Madison, 1101 University Avenue, Madison, WI 53706, USA

Introduction

Gold nanoparticles (AuNPs) have many potential applications in the biomedical and biological fields due to their good chemical stability, high biocompatibility, and the distinct surface plasmon properties (Rosi 2005; Shukla et al. 2005; Jans et al. 2009; Jena 2006; Xu et al. 2011; Sun et al. 2008; Ryan et al. 2007). Large surface-area-to-volume ratio is also another advantage of all the nanocrystals (Daniel and Astruc 2004; Shi et al. 2010a, b, 2011; Boisselier 2009). The physical properties, such as size,

Published online: 25 September 2012

(Lopez-Acevedo et al. 2010; Bao et al. 2007; Alvarez et al. 1997) and shape (Orendorff et al. 2005; Burda et al. 2005; Xia et al. 2009; Nehl and Hafner 2008) of AuNPs determine their optical and electronic properties (Zhou et al. 1999; Bastús et al. 2011; Sánchez-Iglesias et al. 2006). In addition, the chemical properties of AuNPs also correlate to their size (Aikens 2008; Sardar et al. 2009). As a result, controlling the structural and morphological properties of nanoparticles, such as size, shape, and surface chemistry, is important for understanding the optical and electronic properties of metal nanoparticles.

Several methods have been used to synthesize monodisperse AuNPs. In general, the synthesis of AuNPs includes the following steps: reduction, nucleation, and growth (Burda et al. 2005). $NaBH_4$ (Zhou et al. 2010; Sardar and Shumaker-Parry 2011; Torigoe and Esumi 1999) and citrate (Pong et al. 2007; Zhu et al. 2003; Polte et al. 2010a, b; Ojea-Jiménez and Puntes 2009) are two of the most common reduction reagents used for reducing Au ions. 2-[4-(2-hydroxyethyl)-1-piperazinyl] ethanesulfonic acid (HEPES), which usually serves as Good's buffer, is another reduction reagent. HEPES can reduce tetrachloraurate ions by oxidizing their N-substituted piperazine ring to an N-centered cationic free radical (Habib and Tabata 2005; Serizawa and Hirai 2009; Diamanti et al. 2009). In our experiments, we used HEPES to reduce gold precursor solution at room temperature. Right after the reduction process, the Au atoms nucleate and subsequently grow into nanoparticles (Diamanti et al. 2009; Witten and Sander 1981). During the synthesis, nanostructures tend to agglomerate to reduce the overall surface energy. Thus, it is essential to introduce a stabilizer to prevent the nascent nanostructures from agglomerating. Electrostatic stabilization and steric stabilization are two typical stabilization mechanisms (Min et al. 2008). Several chemicals, such as peptide (Panigrahi et al. 2007), monodiperse protein (Housni et al. 2008), amine (Liu et al. 2011), phosphine, carboxylate ligands (Daniel and Astruc 2004), etc., can provide electrostatic stabilization to metal nanoparticles. Though citrate is a reducing reagent, it can also act as a stabilizer, as the negatively charged citrate ions can be electrostatically adsorbed onto nanoparticles (Deka and Paul 2009; Wu et al. 2010; Turkevich et al. 1951). Thiol groups can also stabilize by capping the nanoparticles (Luo et al. 2005; Lin et al. 2004; Daniel and Astruc 2004). In addition, polymers can provide steric stabilization (Sardar and Park 2007).

Gelatin is a natural polymer as well as an edible protein derived from collagen. Owing to its distinct advantages such as low cost, non-toxicity, high affinity to proteins, and good biocompatibility, gelatin is used in a myriad of practical applications (Zhang et al. 2009; Pal 1994; Won et al. 2011; Tielens et al. 2007). Zhang et al. (2009) suggested that amine pendant groups on the gelatin backbone can stabilize the nanoparticles electrostatically; gelatin structure can also provide a steric stabilization. Herein, we report using gelatin as a stabilizer to slow down the process of AuNPs formation at different stages, which allows discerning changes in the system color and better understand the formation mechanisms of AuNPs.

Some researchers have focused on the synthesis and characterization of AuNPs within proteins such as lysozyme, bovine serum albumin, and silk protein, etc., due to their nanoscale structure and various functionalities (Wei et al. 2011; Dickerson et al. 2008). However, to the best of our knowledge, this research is the first in describing the use of gelatin as a stabilizer to slow down the synthesis process of AuNPs and investigate the HEPES-reduced synthesis and growth of AuNPs within gelatin. We also believe that this is the first report on using gelatin as a stabilizer to separate just-aggregated nanoparticles and observe their characteristics.

Based on the observations made with UV–Vis spectra and transmission electron microscopy (TEM), we report that the synthesis of AuNPs within gelatin can be considered to consist of three growth stages. In the earlier stages, the localized surface plasmon resonance (LSPR) peak of AuNPs show a red-shift in UV–Vis spectra, the nucleation happened along with growth which resulted in the increase of size and size dispersion. In the later stage, the LSPR peak of AuNPs red-shifted first and then blue-shifted. When the supply of growth species became much lower, the LSPR peak of AuNPs showed blue-shift only in UV–Vis spectra, during the growth process. We also control the size of the AuNPs by controlling the nucleation time. Moreover, the heating temperature and heating time can also affect the particle sizes. The AuNPs synthesized in gelatin can be used for biomedical and biological applications. For example, two of the widely used applications of gelatin are drug delivery (Olsen et al. 2003; Edwards et al. 1997) and tissue engineering (Li et al. 2006; Ovsianikov et al. 2011; Han et al. 2010). AuNPs can also improve the

cancer treatment (Kennedy et al. 2011; Gobin et al. 2010).

Experimental section

Reagents

Hydrogen tetrachloroaurate (III) trihydrate ($HAuCl_4 \cdot 3H_2O$) and gelatin type A powder were from Acros Organics. 2-[4-(2-hydroxyethyl)-1-piperazinyl] ethanesulfonic acid (HEPES) was purchased from Fisher BioReagents. $HAuCl_4$ 10 mM and HEPES 40 mM (pH 7.2) were prepared in deionized water. $HAuCl_4$ solution was stored in a refrigerator before use. All chemicals and solvents were used without any purification, and all aqueous solutions were prepared in deionized water.

Spectroscopic and microscopic measurements

Absorption spectra (400–700 nm) were measured using Shimadzu UV-1601 PC spectrophotometer. TEM images were obtained using FEI Tecnai T12 transmission electron microscope operating at 80 kV. One drop of sample was placed on a carbon-coated 400 mesh copper grid and excess solution was removed by wicking with filter paper. The grid was allowed to dry at room temperature before imaging. Particle size analysis was performed on at least 100 particles in TEM images using Olympus Soft Imaging Viewer software, and the particle size characteristics (mean and standard deviation) were determined.

Controlling the size of AuNPs by changing the HEPES reduction time

HEPES solution was used to reduce the Au ions at room temperature. However, we controlled the reduction time, the time between mixing $HAuCl_4$ and HEPES solution together and pouring the mixed $HAuCl_4$/HEPES solution into the gelatin solution. As 10 mM $HAuCl_4$ solution was mixed with 40 mM HEPES solution and the mixture was shaken vigorously, the gold precursor ($AuCl_4^-$) was reduced by the oxidation of the N-substituted piperazine ring of HEPES (Habib and Tabata 2005; Diamanti et al. 2009; Serizawa and Hirai 2009). After different reduction times of 60, 70, 80, and 90 s, the mixed solution was poured into the gelatin solution (1 % w/w). These samples are designated as RT60, RT70, RT80, and RT90 samples, respectively. This new mixture of $HAuCl_4$/HEPES/gelatin solutions was placed immediately into a 70 °C hot water bath. Formation and growth of nanoparticles were observed after 3 min. Gelatin powder in the aqueous solution was heterogeneous in the beginning. After heating at 70 °C for 3 min, the gelatin powder dissolved and became a homogeneous gel-like mixture. The size and size dispersion of the resulting AuNPs were determined from TEM analysis.

Heating-time- and heating-temperature-dependent growth of AuNPs

To determine the effect of heating time, RT60, RT70, RT 80, and RT90 samples were heated at 70 °C in a hot water bath for 180 min. During this, small subsamples were drawn periodically every 10 min. The effect of heating temperature was determined by heating RT60 sample in a hot water bath set at 50 and 70 °C for 180 min. The characteristics of AuNPs in all samples were determined by UV–Vis spectra and TEM analysis.

Results and discussion

Effect of reduction time on size of AuNPs

When 10 mM $HAuCl_4$ and 40 mM HEPES were mixed together, the Au ions started to be reduced. The mixed $HAuCl_4$/HEPES solution remained bright yellow for the first 60 s; subsequently, the color became lighter and then transparent for the next 10 s, an indication that most Au ions were reduced to Au atoms during this period. After 80 s of total reduction time, the solution color started to turn violet, suggesting that AuNPs formed and began aggregating. The aggregation is believed to be caused by the van der Waals attraction among the particles (Min et al. 2008). Further aggregation of AuNPs led to dark purple coloration of the system after 90 s. The TEM image of clusters of AuNPs formed in 10 mM $HAuCl_4$/40 mM HEPES mixture after 100 s of reduction time is shown in Fig 1. Since the color of this system was the same as that of RT90 sample (not shown), we presumed that a reduction time of 90 s is sufficient for the synthesized

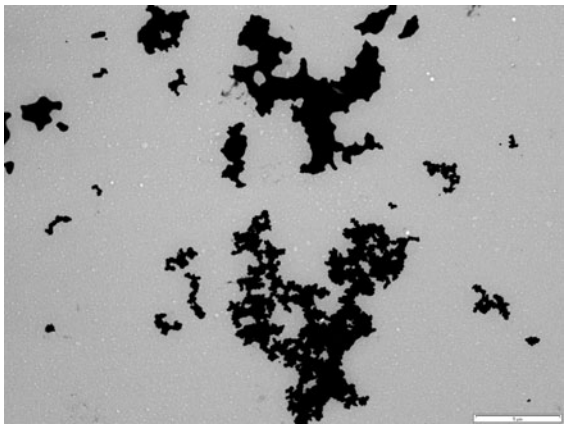

Fig. 1 TEM image of clusters of AuNPs taken at 100 s after mixing (1:1, v/v) 10 mM $HAuCl_4$ and 40 mM HEPES solution. (*scale bar*: 5 μm)

Fig. 2 Color of RT60, RT70, RT80, and RT90 samples (from *left* to *right*, respectively) after heating at 70 °C for 3 min. (Color figure online)

AuNPs to become aggregated. Thus, four samples, each prepared at different reduction times and with different initial colors were chosen: 60 s (bright yellow), 70 s (light yellow), 80 s (violet color just appear), and 90 s (dark purple).

According to Lamer model (LaMer 1950), the nucleation happens when the nuclei concentration becomes larger than a critical value; if the nuclei concentration is smaller, the nuclei disappear. Thus, based on the particle size data, we conclude that in the samples obtained after short reduction times, the nuclei concentration was lower than the critical value to sustain nucleation. Therefore, during the initial reduction time (≤60 s), the $HAuCl_4$/HEPES mixture remained bright yellow. However, when this mixture was poured into the gelatin solution and heated at 70 °C for 3 min, the nucleation started and AuNPs were formed, as noticed by the incipient light pink color (Fig 2) as the result of localized surface plasmon resonance (LSPR) of AuNPs (Ray 2010; Eustis and El-Sayed 2006). It can also be observed in Fig 2 that the color change was more intense in samples that experienced the longer reduction times, when subjected to the same heat treatment. This color difference might attribute to a higher concentration of AuNPs, which the TEM images confirm.

However, as the reduction time was increased, the average particle size decreased from 12.8 ± 2.4 nm (RT60 sample) to 5.1 ± 1.0 nm (RT90 sample) (see Table 1). Gelatin stabilizes AuNPs and slows down the synthesis process at different stages. For the RT60 sample, the AuNPs synthesis was slowed down in its early stage (i.e., nucleation), whereas for the RT90 sample, it was at a later stage (i.e., growth). Thus, the RT60 samples have experienced longer nucleation time, which could possibly explain why the size of AuNPs was larger in RT60 samples, see Scheme 1. Shevchenko and co-workers (Shevchenko et al. 2003) also reported that fast nucleation yielded smaller particles and higher particle concentration while slow nucleation yielded larger particles and lower particle concentration, which our results corroborate.

Table 1 Size and size dispersion of AuNPs synthesized after different durations of HEPES reduction and heating at 70 °C

Reduction time[a] (s)	Heating 3 min Mean (nm) ± SD (%)[b]	Heating 180 min Mean (nm) ± SD (%)[b]
60	12.8 ± 18	17.2 ± 40
70	7.8 ± 13	14.3 ± 26
80	5.1 ± 23	6.1 ± 13
90	5.9 ± 19	5.7 ± 11

SD Standard deviation

[a] Time lapse between mixing 10 mM $HAuCl_4$ and 40 mM HEPES solutions and adding the mixture into 1 % (w/w) gelatin solution

[b] Based on measurements on 100 particles chosen at random

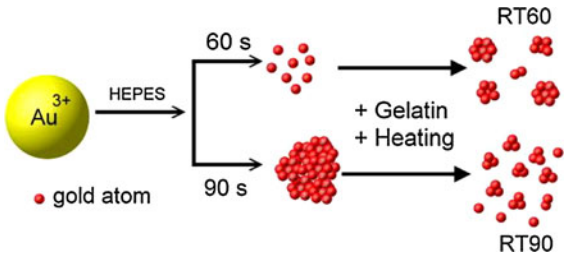

Scheme 1 Gelatin was used to slow down the synthesis of AuNPs at different stages. Samples stabilized at earlier stages (RT60) experienced longer nucleation time, and yielded lager but fewer AuNPs, while the samples stabilized later (RT90), which experienced shorter nucleation time yielded more but smaller AuNPs

The effect of heating time—growth of AuNPs

We followed the growth of AuNPs in $HAuCl_4$/HEPES/gelatin systems described above. For the ease of discussion, based on the status of the AuNPs before the addition of gelatin, we categorized all samples into three groups: (1) pre-aggregation—the reduction time was shorter than when the aggregation of nanoparticles commenced (RT60, RT70), (2) just aggregating—reduction time is the same as when the aggregation commenced (RT80), and (3) post-aggregation—the reduction time was longer than when the aggregation of nanoparticles commenced (RT90).

Pre-aggregation

The initial yellow color indicates that most of the Au ions were not reduced during 60 s of reduction time whereas the light pink color is the result of LSPR of AuNPs (Ray 2010; Eustis and El-Sayed 2006). The UV–Vis spectra indicate a LSPR peak position red-shifted from 526 nm (at 3 min) to 536 nm (at 180 min) during these heating periods (Fig 3a), which might attribute to an increase in the average size of nanoparticles (Sardar and Shumaker-Parry 2011; Polte et al. 2010a, b). The growth of AuNPs was also confirmed by the TEM images (Fig 4). The average size of particles in RT60 samples heated for 3 min is 12.8 nm, while that in samples heated for 180 min is 17.2 nm. However, during that time the size dispersion of AuNPs also increased from 18 to 40 % (see Table 1, Fig 4). The increase in size dispersion implies that, at this stage, new smaller particles are formed along with the growth of existing AuNPs. One possible explanation for these results is that the Au ions continue to be reduced during heating, which increases the nuclei concentration until it exceeds the critical value and initiating nucleation for new particles as well as contributing to particle growth. Zhang et al. (2009) also reported that AuNPs can be synthesized in gelatin solution by heating at 80 °C for 120 min. Similar results of increasing color intensity, particle size, and particle size dispersion with heating time were observed from the RT70 sample (Table 1, Fig 3b).

Relatively speaking, in RT60 and RT70 samples, the effect of gelatin in slowed down the synthesis of AuNPs starts at an earlier stage than in RT80 and RT90 samples. Therefore, in RT60 and RT70 samples the reduction of Au ions happens along with the

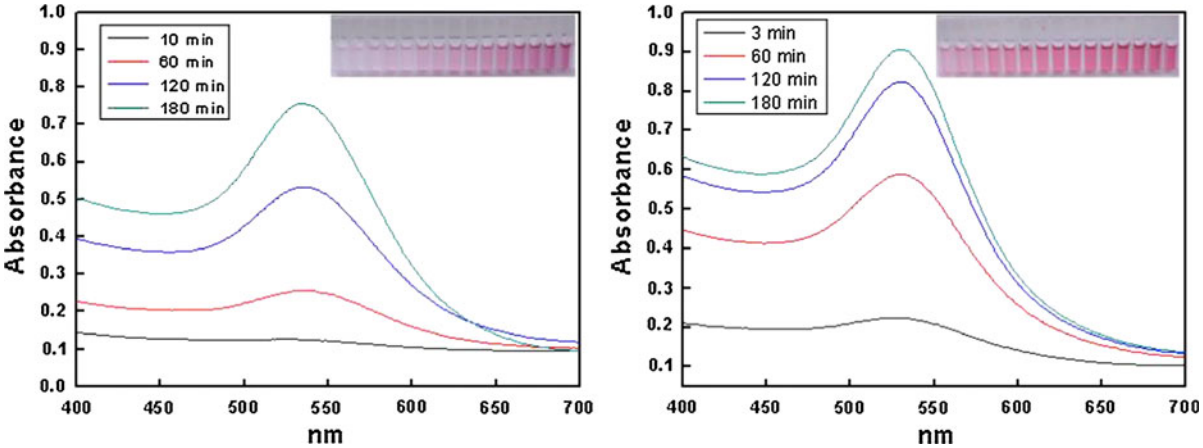

Fig. 3 UV–Vis spectra of (**a**) RT60 and (**b**) RT70 samples at different times during heating at 70 °C. *Insets* show the sample color during heating at 10 min intervals from 10 to 150 min. (Color figure online)

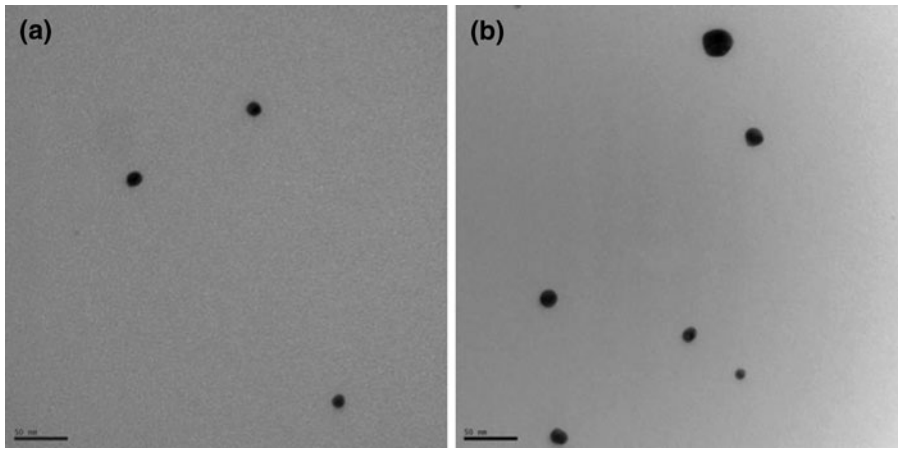

Fig. 4 TEM images of RT60 sample heated at 70 °C for (**a**) 3 min and (**b**) 180 min. (*scale bar*: 50 nm)

nucleation and growth of AuNPs. Heating of RT60 and RT70 samples during these stages tends to increase the size and size dispersion of the AuNPs formed.

Just aggregating

The violet color of RT80 samples result from the aggregation of AuNPs. But, surprisingly, as can be seen in Fig 5e, the LSPR peaks red-shifted from 527 to 528.5 nm during the first 20 min of heating followed by a gradual blue-shift to 523 nm during the next 160 min. The inset in Fig 5e also shows that the sample color became darker during the first 20 min, but remained visually indistinguishable thereafter. The TEM image data show that the particles grew from 5.1 to 6.1 nm from 3 to 20 min, corresponding to the red-shift in the UV–Vis spectra (Sardar and Shumaker-Parry 2011). In general, a blue-shift is associated with a change in the particle crystallinity or dissociation of large particles into smaller ones (Sardar and Shumaker-Parry 2011; Dharmaratne et al. 2009). However, according to the TEM data (Fig 5a–d), while the average particle size remained 6.1 nm during the last 160 min of heating, the size dispersion reduced from 23 to 13 %, see Table 1. Therefore, we attribute the observed blue-shift to the decrease in particle size dispersion. Additional

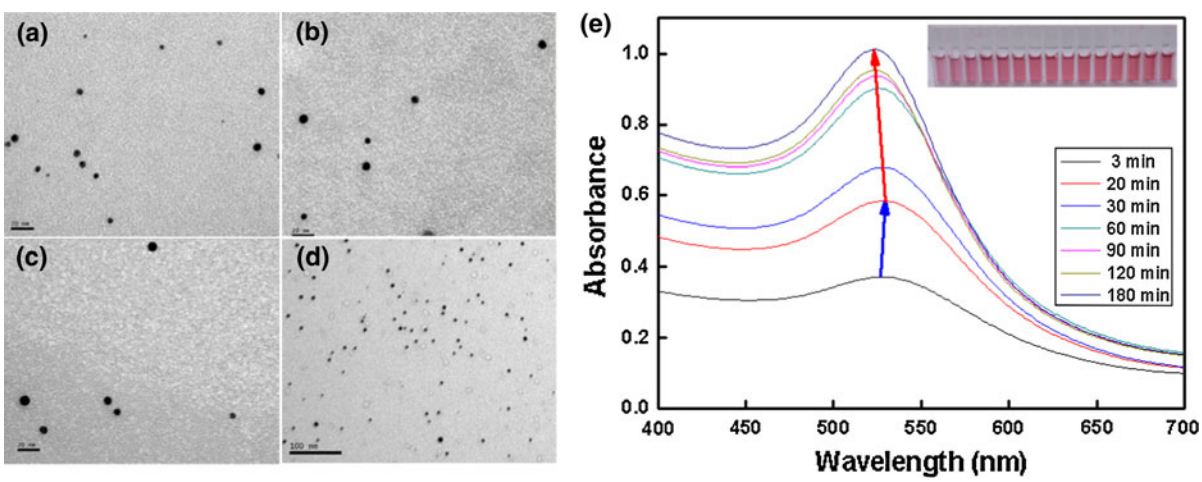

Fig. 5 RT80 samples after heating at 70 °C for (**a**) 3 min, (**b**) 60 min, (**c**) 180 min (*scale bar*: 20 nm) and (**d**) is a lower magnification image at 30 min (*scale bar*: 100 nm). (**e**) UV–Vis spectra of RT80 sample at different times during heating at 70 °C. Inset shows the sample color during heating at 10 min intervals from 10 to 150 min. (Color figure online)

experiments to investigate the changes in crystallinity and structure of the AuNPs are underway to fully understand the reasons for these changes in LSPR.

Most of the smaller particles (<4 nm) observed after 3 min of heating disappeared after 180 min of heating, see Fig 5a–c. This observation may be explained by the diffusion-controlled Ostwald-ripening. Typically, the growth of AuNPs is accelerated by the adsorption of active nuclei on the surface of existing larger particles. Diffusion-limited growth generally happens when the supply of growth species is slow (Sardar and Shumaker-Parry 2011). In our experiments, the stabilizer gelatin, can form a diffusion barrier and hinder the adsorption of nuclei and further growth of nanoparticles. Nonetheless, our results corroborate those of Sardar and Shumaker-Parry (2011), who used 9-orabicyclo[3.3.1]nonane (9-BBN) as a reducing agent to form AuNPs and reported a red-shift followed by a blue-shift in the LSPR peak and attributed the blue-shifting to the decrease in particle size dispersion. They also suggested that this spectral red-shifting followed by blue-shifting occurs when the particle growth follows a classical diffusion-controlled Ostwald-ripening mechanism.

Post-aggregation

As mentioned above, the TEM image conformed the dark purple color in the longer reduction time samples resulted from the aggregation of AuNPs. In this case, the gelatin was also used to separate those aggregated AuNPs. After RT90 sample was poured into gelatin solution, the mixture was shaken vigorously to well-mix the dark purple RT90 solution (just-aggregated AuNPs) and the gelatin solution.

As can be observed from Fig 6, AuNPs from RT90 samples were unaggregated. Further observing the growth of those particles from UV–Vis spectra, the LSPR peak blue-shifted from 534 nm (at 3 min) to 526 nm (at 180 min), see Fig 7. The inset in Fig 7 also shows that the sample color was visually indistinguishable during heating. The TEM images show that while particle size remained almost unchanged (5.7 to 5.9 nm, see Fig 6) during heating, the size dispersion decreased from 19 to 11 % (Table 1), contributing to the blue-shifting. Thus, it appears that gelatin provides not only a steric barrier to prevent further aggregation of AuNPs but also a diffusion barrier to hinder the adsorption of nuclei and further growth of the particles. In this stage, the growth of those separated and isolated AuNPs showed a blue-shift only process, which is correlated to the decrease of size dispersion probably due to diffusion-controlled Ostwald-ripening mechanism.

Temperature-dependent growth of AuNPs

Table 2 shows how temperature influences the size of AuNPs synthesized in gelatin. We chose RT60 (pre-aggregation) sample for observing temperature-dependent growth because the sample color is distinguishable to the naked eyes during the heating period. The average particle sizes after heating the RT60 sample for 3 and 180 min were 12.5 and 15.1 nm, respectively, at 50 °C; and 12.8 and 17.2 nm, respectively, at 70 °C. The LSPR peak positions of UV–Vis spectra of both sets of samples were similar (Fig 8), consistent with the similarities of their size (12.5 and 12.8 nm). However, after 180 min of heating, the amplitude of the spectrum of sample heated at 70 °C was higher than that was heated at 50 °C, which indicated

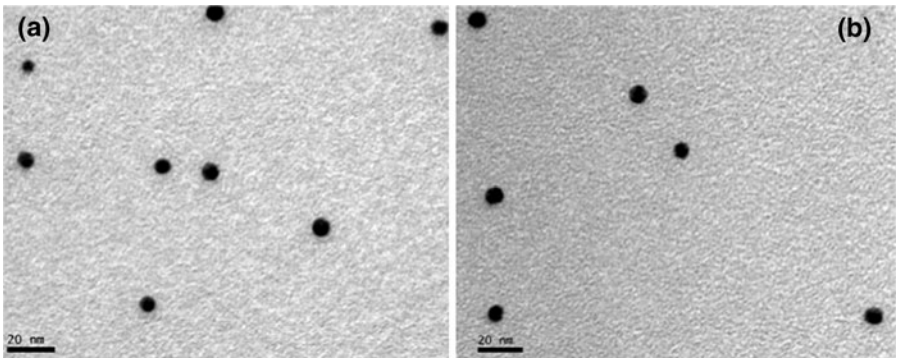

Fig. 6 TEM images of RT90 sample after heating at 70 °C for (**a**) 3 min and (**b**) 180 min. (*scale bar*: 20 nm)

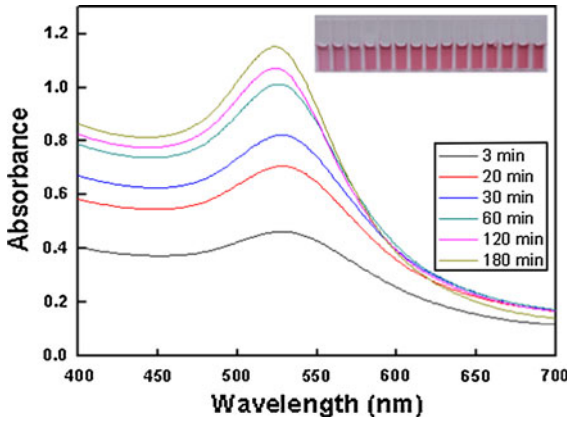

Fig. 7 UV–Vis spectra of RT90 sample at different times during heating at 70 °C. *Inset* shows the sample color during heating at 10 min intervals from 10 to 150 min. (Color figure online)

Table 2 Size and size dispersion of AuNPs synthesized[a] by heating for different duration at different temperatures

Heating Temperature (°C)	Heating 3 min Mean (nm) ± SD (%)[b]	Heating 180 min Mean (nm) ± SD (%)[b]
50	12.5 ± 14	15.1 ± 16
70	12.8 ± 18	17.2 ± 40

[a] Time lapse between mixing 10 mM $HAuCl_4$ and 40 mM HEPES solutions and adding the mixture to into 1 % (w/w) gelatin solution was 60 s

[b] Based on measurements on 100 particles chosen at random

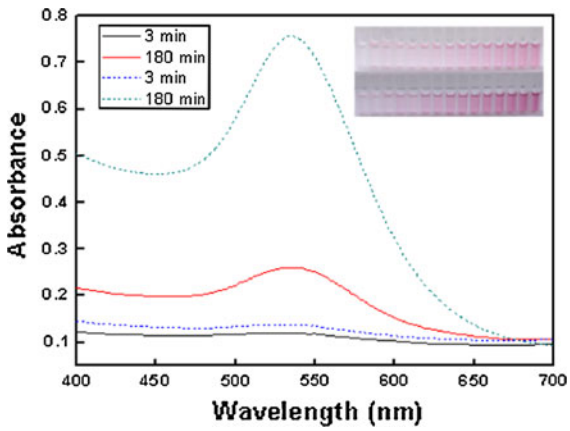

Fig. 8 UV–Vis spectra of RT60 sample after heating at different temperatures (*line*: 50 °C; *dash*: 70 °C) for different durations. Inset shows the sample color during heating at different temperatures (*top row*: 50 °C; *bottom row*: 70 °C) at 10 min intervals from 10 to 150 min. (Color figure online)

that more nanoparticles were synthesized at 70 °C (Sardar and Shumaker-Parry 2011). This might result from the reduction of Au ions by gelatin molecules at higher temperature (Zhang et al. 2009). The larger size dispersion obtained at 70 °C also confirmed these results, see table 2. In addition, the color of the sample heated at 70 °C was darker than that was heated at 50 °C, see inset in Fig 8. Because the color of the sample is correlated with temperature, this technique might be applied as a temperature indicator.

Conclusions

We used gelatin as a stabilizer to slow down the formation of AuNPs, which enabled investigating the effect of experimental parameters on the size and size dispersion of AuNPs. Based on the observations of TEM analysis and UV–Vis spectra, we report that the synthesis of HEPES-reduced AuNPs within gelatin can be considered to consist of three growth stages. First, during the initial stage, the reduction of gold precursor occurred along with nucleation and growth, which resulted in a red-shift phenomenon of LSPR peak of AuNPs in UV–Vis spectra (size and size dispersion increase). Second, the LSPR peak of AuNPs in UV–Vis spectra showed first red-shift and then blue-shift during the growth of AuNPs. According to the TEM analysis, the blue-shift might be due to the diffusion-limited Ostwald-ripening mechanism. Third, the LSPR peak showed blue-shift only during the growth of AuNPs. We also demonstrated that limiting the duration that $HAuCl_4$ is reduced by HEPES, by adding the $HAuCl_4$/HEPES mixture into gelatin solution, allows slowing the synthesis of AuNPs at an earlier stage (nucleation stage). If the $HAuCl_4$/HEPES/gelatin system has a longer nucleation time during the formation of AuNPs, fewer but larger AuNPs are formed; however, if the samples experienced shorter nucleation time, the AuNPs formed are smaller but more numerous. Allowing enough time for HEPES reduction of $HAuCl_4$ and by adding the $HAuCl_4$/HEPES mixture into gelatin solution such that the aggregation of AuNPs had already happened, the growth of AuNPs would be limited by diffusion-controlled Ostwald-ripening, which was confirmed by the TEM and UV–Vis spectroscopy. If the supply of growth species (Au precursor) becomes lower, in the case of longer

reduction samples, the polymer structure of gelatin might hinder the diffusion as well as the adsorption and further growth of the nanoparticles. Moreover, the heating time and temperature also influence the size of AuNPs. By controlling the reduction time, heating temperature and heating time, AuNPs of average size of 5–17 nm can be synthesized. In the heating temperature range of 50–70 °C, the color of the $HAuCl_4$/HEPES/gelatin samples showed different intensities. Longer heating times resulted in larger average particle sizes and the sample color was darker. These results imply that the $HAuCl_4$/HEPES/gelatin system can be potentially used as a temperature indicator. Further investigations could help to understand the synthesis process of AuNPs. For example, selected area electron diffraction (SAED), small angle X-ray scattering (SAXS), and in situ characterization of AuNP crystallinity can provide additional information on the process of AuNPs formation. These results could form a basis for tuning the size, size dispersion of AuNPs, and monitor the process of their synthesis.

Acknowledgments We thank Jay Campbell of Department of Biochemistry at University of Wisconsin-Madison for his assistance with acquiring TEM images.

References

Aikens C (2008) Origin of discrete optical absorption spectra of M25 (SH) 18−nanoparticles (M = Au, Ag). J Phy Chem C 112(50):19797–19800

Alvarez M, Khoury J, Schaaff T (1997) Optical absorption spectra of nanocrystal gold molecules. J Phy Chem B 101:3706–3712

Bao Y, Zhong C, Vu D, Temirov J (2007) Nanoparticle-free synthesis of fluorescent gold nanoclusters at physiological temperature. J Phys Chem C 111(33):12194–12198

Bastús NG, Comenge J, Puntes Vc (2011) Kinetically controlled seeded growth synthesis of citrate-stabilized gold nanoparticles of up to 200 nm: size focusing versus Ostwald ripening. Langmuir 27(17):11098–11105

Boisselier E (2009) Gold nanoparticles in nanomedicine: preparations, imaging, diagnostics, therapies and toxicity. Chem Soc Rev 38:1759–1782

Burda C, Chen X, Narayanan R (2005) Chemistry and properties of nanocrystals of different shapes. Chem Rev 105:1025–1102

Daniel M-C, Astruc D (2004) Gold nanoparticles: assembly, supramolecular chemistry, quantum-size-related properties, and applications toward biology, catalysis, and nanotechnology. Chem Rev 104(1):293–346

Deka J, Paul A (2009) Sensitive protein assay with distinction of conformations based on visible absorption changes of citrate-stabilized gold nanoparticles. J Phy Chem C 115 (32):15752–15757

Dharmaratne AC, Krick T, Dass A (2009) Nanocluster size evolution studied by mass spectrometry in room temperature Au25(SR)18 synthesis. J Am Chem Soc 131(38): 13604–13605

Diamanti S, Elsen A, Naik R (2009) Relative functionality of buffer and peptide in gold nanoparticle formation. J Phy Chem C 113(23):9993–9997

Dickerson MB, Sandhage KH, Naik RR (2008) Protein- and peptide-directed syntheses of inorganic materials. Chem Rev 108(11):4935–4978

Edwards DA, Hanes J, Caponetti G, Hrkach J, Ben-Jebria A, Eskew ML, Mintzes J, Deaver D, Lotan N, Langer R (1997) Large porous particles for pulmonary drug delivery. Science 276(5320):1868–1872

Eustis S, El-Sayed MA (2006) Why gold nanoparticles are more precious than pretty gold: noble metal surface plasmon resonance and its enhancement of the radiative and nonradiative properties of nanocrystals of different shapes. Chem Soc Rev 35(3):209–217

Gobin AM, Watkins EM, Quevedo E, Colvin VL, West JL (2010) Near-infrared-resonant gold/gold sulfide nanoparticles as a photothermal cancer therapeutic agent. Small 6(6):745–752

Habib A, Tabata M (2005) Formation of gold nanoparticles by goods buffers. Bull Chem Soc Jpn 78(2):262–269

Han J, Lazarovici P, Pomerantz C, Chen X, Wei Y, Lelkes PI (2010) Co-electrospun blends of PLGA, gelatin, and elastin as potential nonthrombogenic scaffolds for vascular tissue engineering. Biomacromolecules 12(2):399–408

Housni AAM, Liu S, Narain R (2008) Monodisperse protein stabilized gold nanoparticles via a simple photochemical process. J Phys Chem C 112(32):12282–12290

Jans H, Liu X, Austin L, Maes G, Huo Q (2009) Dynamic light scattering as a powerful tool for gold nanoparticle bioconjugation and biomolecular binding studies. Anal Chem 81(22):9425–9432

Jena B (2006) Electrochemical biosensor based on integrated assembly of dehydrogenase enzymes and gold nanoparticles. Anal Chem 78(18):6332–6339

Kennedy LC, Bickford LR, Lewinski NA, Coughlin AJ, Hu Y, Day ES, West JL, Drezek RA (2011) A new era for cancer treatment: gold-nanoparticle-mediated thermal therapies. Small 7(2):169–183

LaMer KDRH (1950) Theory, production and mechanism of formation of monodispersed hydrosols. J Am Chem Soc 72:4847–4857

Li M, Guo Y, Wei Y, MacDiarmid AG, Lelkes PI (2006) Electrospinning polyaniline-contained gelatin nanofibers for tissue engineering applications. Biomaterials 27(13): 2705–2715

Lin S-Y, Tsai Y-T, Chen C-C, Lin C-M, Chen C-H (2004) Two-step functionalization of neutral and positively charged thiols onto citrate-stabilized Au nanoparticles. J Phys Chem B 108(7):2134–2139

Liu G, Luais E, Gooding JJ (2011) The fabrication of stable gold nanoparticle-modified interfaces for electrochemistry. Langmuir 27(7):4176–4183

Lopez-Acevedo O, Tsunoyama H, Tsukuda T, Häkkinen H, Aikens CM (2010) Chirality and electronic structure of the

thiolate-protected Au38 nanocluster. J Am Chem Soc 132(23):8210–8218
Luo S, Xu J, Zhang Y, Liu S, Wu C (2005) Double hydrophilic block copolymer monolayer protected hybrid gold nanoparticles and their shell cross-linking. J Phys Chem B 109(47):22159–22166
Min Y, Akbulut M, Kristiansen K, Golan Y, Israelachvili J (2008) The role of interparticle and external forces in nanoparticle assembly. Nat Mater 7(7):527–538
Nehl CL, Hafner JH (2008) Shape-dependent plasmon resonances of gold nanoparticles. J Mater Chem 18(21):2415
Ojea-Jiménez I, Puntes V (2009) Instability of cationic gold nanoparticle bioconjugates: the role of citrate ions. J Am Chem Soc 131(37):13320–13327
Olsen D, Yang C, Bodo M, Chang R (2003) Advanced drug delivery reviews : recombinant collagen and gelatin for drug delivery. Adv Drug Deliv Rev 55(12):1547–1567
Orendorff C, Gole A, Sau T (2005) Surface-enhanced Raman spectroscopy of self-assembled monolayers: sandwich architecture and nanoparticle shape dependence. Anal Chem 77(10):3261–3266
Ovsianikov A, Deiwick A, van Vlierberghe S, Dubruel P, Möller L, Dräger G, Chichkov B (2011) Laser fabrication of three-dimensional CAD scaffolds from photosensitive gelatin for applications in tissue engineering. Biomacromolecules 12(4):851–858
Pal T (1994) Gelatin-A compound for all reasons. J Chem Educ 71(8):679
Panigrahi S, Kundu S, Basu S, Praharaj S, Jana S, Pande S, Ghosh SK, Pal A, Pal T (2007) Nonaqueous route for the synthesis of copper organosol from copper stearate: an effective catalyst for the synthesis of octylphenyl ether. J Phys Chem C 111(4):1612–1619
Polte J, Ahner TT, Delissen F, Sokolov S, Emmerling F, Thnemann AF, Kraehnert R (2010a) Mechanism of gold nanoparticle formation in the classical citrate synthesis method derived from coupled in situ XANES and SAXS evaluation. J Am Chem Soc 132(4):1296–1301
Polte J, Erler R, Thünemann AF, Sokolov S, Ahner TT, Rademann K, Emmerling F, Kraehnert R (2010b) Nucleation and growth of gold nanoparticles studied via in situ small angle X-ray scattering at millisecond time resolution. ACS Nano 4(2):1076–1082
Pong B-K, Elim HI, Chong JX, Ji W, Trout BL, Lee JY (2007) New insights on the nanoparticle growth mechanism in the citrate reduction of gold(III) salt: formation of the Au nanowire intermediate and its nonlinear optical properties. J Phys Chem C 111(17):6281–6287
Ray PC (2010) Size and shape dependent second order nonlinear optical properties of nanomaterials and their application in biological and chemical sensing. Chem Rev 110(9): 5332–5365
Rosi N (2005) Nanostructures in biodiagnostics. Chem Rev 105(1):1547–1562
Ryan JA, Overton KW, Speight ME, Oldenburg CN, Loo L, Robarge W, Franzen S, Feldheim DL (2007) Cellular uptake of gold nanoparticles passivated with BSA-SV40 large T antigen conjugates. Anal Chem 79(23):9150–9159
Sánchez-Iglesias A, Pastoriza-Santos I, Pérez-Juste J, Rodríguez-González B, García de Abajo FJ, Liz-Marzán LM (2006) Synthesis and optical properties of gold nanodecahedra with size control. Adv Mater 18(19):2529–2534
Sardar R, Park J (2007) Polymer-induced synthesis of stable gold and silver nanoparticles and subsequent ligand exchange in water. Langmuir 23(23):11883–11889
Sardar R, Shumaker-Parry JS (2011) Spectroscopic and microscopic investigation of gold nanoparticle formation: ligand and temperature effects on rate and particle size. J Am Chem Soc 133(21):8179–8190
Sardar R, Funston A, Mulvaney P (2009) Gold nanoparticles: past, present, and future. Langmuir 25(24):13840–13851
Serizawa T, Hirai Y (2009) Novel synthetic route to peptide-capped gold nanoparticles. Langmuir 25(20):12229–12234
Shevchenko EV, Talapin DV, Schnablegger H, Kornowski A, Festin Ö, Svedlindh P, Haase M, Weller H (2003) Study of nucleation and growth in the organometallic synthesis of magnetic alloy nanocrystals: the role of nucleation rate in size control of CoPt3 nanocrystals. J Am Chem Soc 125(30):9090–9101
Shi L, Pei C, Li Q (2010a) Fabrication of ordered single-crystalline CuInSe2 nanowire arrays. CrystEngComm 12(11):3882–3885
Shi L, Pei C, Li Q (2010b) Ordered arrays of shape tunable CuInS2 nanostructures, from nanotubes to nano test tubes and nanowires. Nanoscale 2(10):2126–2130
Shi L, Pei C, Xu Y, Li Q (2011) Template-directed synthesis of ordered single-crystalline nanowires arrays of Cu_2ZnSnS_4 and $Cu_2ZnSnSe_4$. J Am Chem Soc 133(27):10328–10331
Shukla R, Bansal V, Chaudhary M, Basu A (2005) Biocompatibility of gold nanoparticles and their endocytotic fate inside the cellular compartment: a microscopic overview. Langmuir 21(23):10644–10654
Sun L, Liu D, Wang Z (2008) Functional gold nanoparticle-peptide complexes as cell-targeting agents. Langmuir 24(18):10293–10297
Tielens S, Declercq H, Gorski T, Lippens E, Schacht E, Cornelissen M (2007) Gelatin-based microcarriers as embryonic stem cell delivery system in bone tissue engineering: an in vitro study. Biomacromolecules 8(3):825–832
Torigoe K, Esumi K (1999) Preparation and catalytic effect of gold nanoparticles in water dissolving carbon disulfide. J Phys Chem B 103(15):2862–2866
Turkevich J, Stevenson PC, Hillier J (1951) A study of the nucleation and growth processes in the synthesis of colloidal gold. Discuss Faraday Soc 11:55–75
Wei H, Wang Z, Zhang J, House S, Gao Y-G, Yang L, Robinson H, Tan LH, Xing H, Hou C, Robertson IM, Zuo J-M, Lu Y (2011) Time-dependent, protein-directed growth of gold nanoparticles within a single crystal of lysozyme. Nat Nanotechnol 6(2):93–97
Witten T Jr, Sander L (1981) Diffusion-limited aggregation, a kinetic critical phenomenon. Phys Rev Lett 47(19):1400–1403
Won Y-W, Yoon S-M, Sonn CH, Lee K-M, Kim Y-H (2011) Nano self-assembly of recombinant human gelatin conjugated with α-tocopheryl succinate for Hsp90 inhibitor, 17-AAG delivery. ACS Nano 5(5):3839–3848
Wu X, Thrall E, Liu H (2010) Plasmon induced photovoltage and charge separation in citrate-stabilized gold nanoparticles. J Phy Chem C 114(30):12896–12899

Xia Y, Xiong Y, Lim B, Skrabalak SE (2009) Shape-controlled synthesis of metal nanocrystals: simple chemistry meets complex physics? Angew Chem Int Ed 48(1):60–103

Xu LG, Zhu YY, Ma W, Chen W, Liu L, Kuang H, Wang L, Xu C (2011) New synthesis strategy for DNA functional gold nanoparticles. J Phys Chem C 115(8):3243–3249

Zhang J-J, Gu M-M, Zheng T-T, Zhu J-J (2009) Synthesis of gelatin-stabilized gold nanoparticles and assembly of carboxylic single-walled carbon nanotubes/Au composites for cytosensing and drug uptake. Anal Chem 81(16): 6641–6648

Zhou Y, Wang C, Zhu Y (1999) A novel ultraviolet irradiation technique for shape-controlled synthesis of gold nanoparticles at room temperature. Chem Mater 11(9):2310–2312

Zhou CSC, Yu M, Qin Y, Wang J, Kim M, Zheng J (2010) Luminescent gold nanoparticles with mixed valence states generated from dissociation of polymeric Au(I) thiolates. J Phys Chem C 114(17):7727–7732

Zhu T, Vasilev K, Kreiter M, Mittler S (2003) Surface modification of citrate-reduced colloidal gold nanoparticles with 2-mercaptosuccinic acid. Langmuir 19(22):9518–9525